Photocatalysis

Deutsche Ausgabe: DOI: 10.1002/ange.201605367
Internationale Ausgabe: DOI: 10.1002/anie.201605367

Unique Electronic Structure in a Porous Ga-In Bimetallic Oxide Nano-Photocatalyst with Atomically Thin Pore Walls

Hui Chen[+], Guangtao Yu[+], Guo-Dong Li, Tengfeng Xie, Yuanhui Sun, Jingwei Liu, Hui Li, Xuri Huang, Dejun Wang, Tewodros Asefa, Wei Chen,* and Xiaoxin Zou**

Abstract: *A facile synthetic route is presented that produces a porous Ga-In bimetallic oxide nanophotocatalyst with atomically thin pore walls. The material has an unprecedented electronic structure arising from its ultrathin walls. The bottom of the conduction band and the top of the valence band of the material are distributed on two opposite surfaces separated with a small electrostatic potential difference. This not only shortens the distance by which the photogenerated charges travel from the sites where they are generated to the sites where they catalyze the reactions, but also facilitates charge separations in the material. The porous structure within the walls results in a large density of exposed surface reactive/catalytic sites. Because of these optimized electronic and surface structures, the material exhibits superior photocatalytic activity toward the hydrogen evolution reaction (HER).*

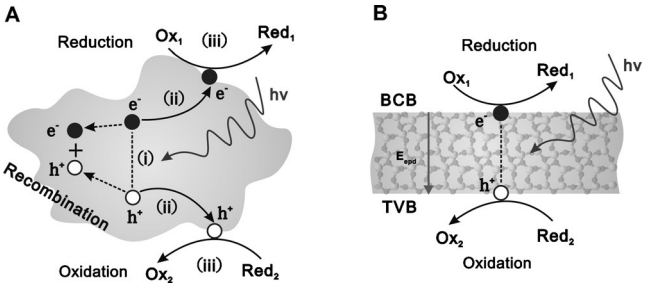

Figure 1. A) Some of the key processes involved in semiconductor photocatalysis. B) A proposed nanophotocatalyst with atomically thin pore walls and the photocatalytic processes expected to undergo in it. Red and Ox denote oxidized and reduced species, respectively. BCB and TVB represent the bottom of a conduction band and the top of a valence band, respectively. E_{epd} represents the electrostatic potential difference between BCB and TVB.

Photocatalysis has long been considered one of the most promising routes to provide synthetic fuels from renewable sources in a sustainable way.[1] At the heart of photocatalysis are materials called photocatalysts, which have the ability to capture light and use the light to facilitate chemical conversions. Photocatalysis generally involves three key processes (Figure 1 A):[2] 1) light absorption, followed by generation of electron-hole pairs (also known as excitons or charge carriers); 2) separation of charge carriers, followed by charge migration to the photocatalyst surfaces; and 3) chemical conversion of adsorbate molecules on the photocatalyst surface with the charge carriers. While the light absorption and carrier transport processes are closely linked to the electronic structures of the photocatalyst, the surface chemical reactions and inhibition of carrier recombination rely largely on the photocatalyst surface structures.[3,4] Hence, for a material to be an ideal photocatalyst, it has to have optimized electronic as well as surface structures that can promote the aforementioned three key photocatalytic processes while simultaneously suppressing photoexcited charge carrier recombination.

To this end, we conceptually hypothesized that these kinds of photocatalysts could be realized by making porous semiconducting nanofibers with atomically thin pore walls (Figure 1 B). Such nanostructure should result in synergistically optimized electronic and surface properties, and thereby significantly enhanced photocatalytic activity in the material. In particular, the atomically thin pore walls might generate an unprecedented electronic structure in the material by making the bottom of its conduction band and the top of its valence band to be distributed on opposite sides of the material with some electrostatic potential difference. This type of electronic structure can, in turn, facilitate the separation of charge carriers, besides minimizing the distances that the photogenerated charges have to travel from the sites they are generated to reach to the sites they catalyze the reactions.[5] Furthermore, the porous structure, together with the ultrathin pore walls, can render such materials a large density of catalytically active sites exposed to reactants.

[*] H. Chen,[+] Prof. G.-D. Li, Prof. T. Xie, Prof. D. Wang, Prof. X. Zou
State Key Laboratory of Inorganic Synthesis and Preparative Chemistry, International Joint Research Laboratory of Nano-Micro Architecture Chemistry, College of Chemistry, Jilin University
Changchun 130012 (P.R. China)
E-mail: xxzou@jlu.edu.cn

Prof. G. Yu,[+] Y. Sun, J. Liu, H. Li, Prof. X. Huang, Prof. W. Chen
Institute of Theoretical Chemistry, International Joint Research Laboratory of Nano-Micro Architecture Chemistry, Jilin University
Changchun 130023 (P.R. China)
E-mail: xychwei@gmail.com

Prof. T. Asefa
Department of Chemistry and Chemical Biology & Department of Chemical and Biochemical Engineering
Rutgers, The State University of New Jersey
Piscataway, NJ 08854 (USA)
E-mail: tasefa@rci.rutgers.edu

H. Chen[+]
Department of Materials Science and Engineering, Jilin University
Changchun 130022 (P.R. China)

Prof. D. Wang
Department of Chemistry, Tsinghua University
Beijing 100084 (P.R. China)

[+] These authors contributed equally to this work.

Supporting information for this article can be found under: http://dx.doi.org/10.1002/anie.201605367.

To demonstrate this idea, we chose β-Ga_2O_3, which has been studied for photocatalysis (for example, the hydrogen evolution reaction and decomposition of organic pollutants).[6] Several theoretical and experimental studies showed that the photocatalytic activity of β-Ga_2O_3 could be improved by doping it with other elements or introducing in it surface heterostructures.[7] However, as the previously reported β-Ga_2O_3 materials had relatively low surface areas and inherently limited exposed reactive sites, the improvements in catalytic performance achieved in them were suboptimal. Conversely, β-Ga_2O_3-based materials with atomically thin structures, which can potentially generate electronically confined structures and much higher photocatalytic activity, have never been realized or demonstrated so far.

Herein we report, for the first time, a facile synthetic route that produces novel porous In-doped β-Ga_2O_3 nanofibers (dubbed $Ga_xIn_yO_3$, where $x+y=2$ and $1.8\geq x\geq 1.0$) with atomically thin pore walls and excellent photocatalytic properties. This work also demonstrates the realization of our conceptual idea above, namely that porous nanophotocatalysts with atomically thin pore walls would constitute optimized electronic and surface structures, and thereby high photocatalytic activity.

The synthesis of $Ga_xIn_yO_3$ involves two major steps (see the Supporting Information for details): 1) synthesis of Ga- and In-embedded polyvinylpyrrolidone (PVP) nanofibers (the precursors) via an electrospinning method (Figure S1) and 2) thermal treatment of the Ga- and In-embedded PVP nanofibers in air at 600 °C. Among the many possible $Ga_xIn_yO_3$ we tried to synthesize, $Ga_{1.7}In_{0.3}O_3$ has been found to show the best catalytic activity, and thus most of the characterizations and discussions here focus on this particular material.

The typical scanning electron microscopy (SEM) image of $Ga_{1.7}In_{0.3}O_3$ (Figure 2A) reveals that this material has a 1D nanofiber-like morphology, with a length of several μm and a width of 50–150 nm. Further analysis by transmission electron microscopy (TEM) indicates that the material has a highly porous foam-like nano-network structure (Figure 2B,C). The presence of porosity in the material is confirmed by N_2 porosimetry (Supporting Information, Figure S2). The latter further reveals the co-presence of mesopores and macropores and a BET surface area of ca. 35 m^2g^{-1} in the material. TEM images (for example, Figure 2C) show that the pores in the material are built from randomly but spatially interconnected ultrathin nanosheet walls. High-resolution TEM (HRTEM) images (Figures 2D,E; Supporting Information, Figure S3) indicate that the thickness of the ultrathin pore walls is 0.85–2.00 nm. Parallel to the pore walls, lattice fringes (0.282 nm in dimension) exist that can be attributed to the (002) crystallographic planes of $Ga_{1.7}In_{0.3}O_3$. These results imply that the exposed facets in the ultrathin pore walls are of the (002) type. The ultrathin pore walls as seen to contain 3–7 atomic layers, with 5 atomic layers being the most prominent one (Supporting Information, Figure S4). Additionally, elemental mapping of the material shows that all the elements, that is, Ga, In, and O, are homogeneously distributed at the nanoscale over the entire $Ga_{1.7}In_{0.3}O_3$ nanofibers. It is worth emphasizing here that such a type of

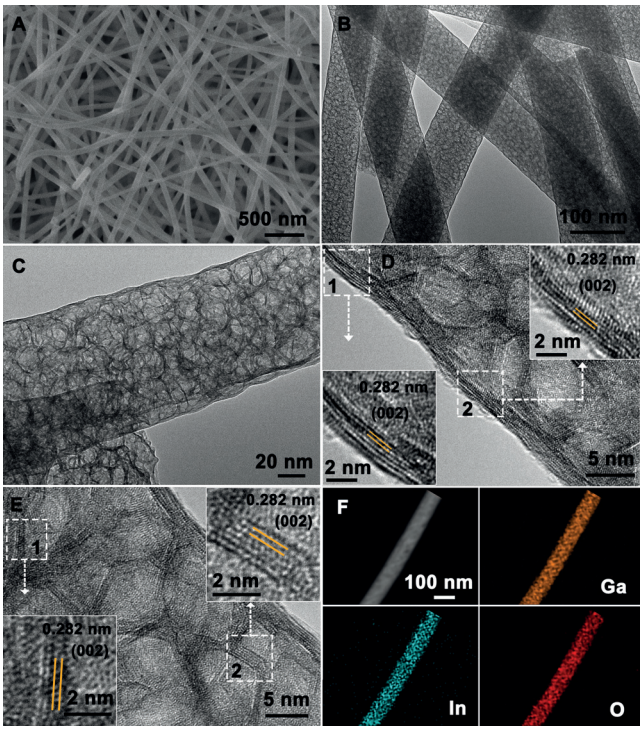

Figure 2. A) SEM image, B),C) TEM images, and D),E) HRTEM images of $Ga_{1.7}In_{0.3}O_3$. F) A scanning transmission electron microscopy (STEM) image of $Ga_{1.7}In_{0.3}O_3$ and the corresponding elemental mapping images of the different elements present in the material.

nanomaterial with atomically thin pore walls have not been reported for Ga-/In-oxides before. Notably also, attempted synthesis using other dopants, such as Zn, Cd, Fe, and Al, failed to generate porous metal-substituted β-Ga_2O_3 nanofibers with atomically thin pore walls (Supporting Information, Figure S5). This indicates that In is unique in its ability to generate the type of ultrathin walled In-doped Ga_2O_3 nanomaterial reported here.

Furthermore, the porous $Ga_xIn_yO_3$ nanofibers with atomically thin pore walls form only with Ga:In atomic ratios ranging from 1.0:1.0 to 1.8:0.2 in the precursor (Figure 2). When the Ga:In atomic ratio is lower than 1.0:1.0, Ga-doped In_2O_3 nanofibers comprising densely packed nanoparticles form instead (Supporting Information, Figures S6 and S7). On the other hand, when the Ga:In atomic ratio is larger than 1.8:0.2, β-Ga_2O_3 nanotubes form with walls having more than 8 atomic layers possessing some nanoparticles in their inner parts (Supporting Information, Figure S8). The crystal structures adopted by the materials prepared from different Ga:In ratios here are in agreement with those formed by bulk Ga- and In-based bimetallic oxides.[8] The above results also indicate that the presence of a certain amount of In dopants significantly alters the nanoscale morphology of β-Ga_2O_3, something that has also never been reported for Ga-In bimetallic oxides before.

To further assess the structure of the ultrathin pore walls of $Ga_xIn_yO_3$, detailed theoretical studies are performed (Supporting Information, Figures S9–S11). Specifically, two basic questions are posed: 1) where do the In dopants reside

in the ultrathin pore walls and 2) why do the pore walls prefer to take a 5 atomic-layer-thick ultrathin wall? To answer the first question, the structural models of β-Ga_2O_3 with 5 atomic layers are constructed, and then the substituted energy (E_{sub}) of In atoms at any possible Ga sites in the models is determined. Interestingly, the computed results reveal that the prominent, 5 atomic-layer β-Ga_2O_3 nanosheet has two different exposed surfaces, denoted as surface-1′ and surface 2′, possessing intrinsic compressive and tensile strains, respectively (Supporting Information, Figure S10 and discussion therein). Owing to these differences in strain, the In dopant atoms, which are larger in size than Ga atoms, tend to replace the Ga atoms in surface-2′. This is revealed by the fact that the E_{sub} values in the surface-2′ are much lower than those in other four atomic layers (Figure 3 A) as well as those in bulk β-Ga_2O_3.

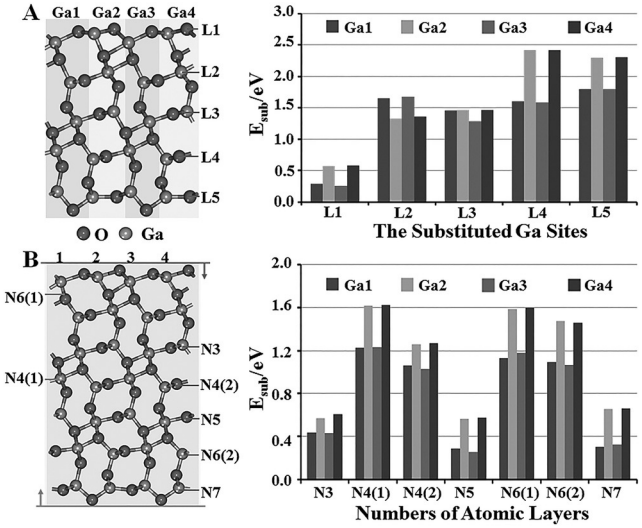

Figure 3. A) Effect of the location of In dopant atoms (Ga-1 to Ga-4 at different layers, L1 to L5) on the value of E_{sub} in the 5 atomic layer-thin β-Ga_2O_3 nanosheet. B) Effect of the number of atomic layer on the value of E_{sub} for β-Ga_2O_3 nanosheets, where several thicknesses with odd and even layers are sampled, namely three (N3), five (N5), and seven (N7) layers and four (N4(1) and N4(2)) and six (N6(1) and N6(2)) layers. The numbers 1 and 2 in parenthesis indicate surface-1 and surface-2, respectively (see also the Supporting Information, Figure S8).

After determining the location of In dopants in the ultrathin pore walls, we examined why the ultrathin pore walls with five-atomic-layers is favored in $Ga_{1.7}In_{0.3}O_3$. For this, four more structural models of β-Ga_2O_3 nanosheets with three, four, six, and seven atomic-layers are constructed (Supporting Information, Figure S11), and the effect of the number of atomic layers on the value of E_{sub} of In dopants is investigated. Note that the nanosheets have two similar surfaces when the atomic-layers are even (that is, four and six) but have different surfaces when the atomic-layers are odd (that is, three, five, and seven). The values of E_{sub} for In dopants for these nanosheets are evaluated by replacing Ga atoms with In dopant atoms (Supporting Information). Figure 3 B shows the comparison of the computed E_{sub} of In dopants as a function of the number of atomic layers in the nanosheets, from which two conclusions can be made: 1) the E_{sub} values (1.028–1.620 eV) for the even atomic-layered nanosheets are much larger than those for the odd atomic-layered nanosheets (0.256–0.661 eV), owing primarily to the absence of tensile strain at the surfaces of the even-layered structures; and 2) for the odd-layered nanosheets, the E_{sub} values are the smallest for the 5 atomic-layer nanosheet owing to its most favorable tensile strain. These might also well be the reasons behind the preferred formation of 5 atomic-layer-thin pore walls in $Ga_xIn_yO_3$.

As the electronic structures of photocatalytically active materials dictate their catalytic performances (as mentioned above), the total density of states (TDOS) and local density of states (LDOS) of $Ga_{1.7}In_{0.3}O_3$ possessing unique ultrathin pore walls are computed. For comparison, the TDOS and LDOS of structurally relevant bulk β-Ga_2O_3 are also computed. The results (Figure 4 A) reveal that the conduction band of $Ga_{1.7}In_{0.3}O_3$ is lower in energy than that of bulk β-Ga_2O_3, but the valence band of $Ga_{1.7}In_{0.3}O_3$ is equal in energy as that of bulk β-Ga_2O_3. The results also suggest that the band gap in β-Ga_2O_3 decreases upon doping with In atoms, in good agreement with experimental results (Supporting Information, Figure S12).

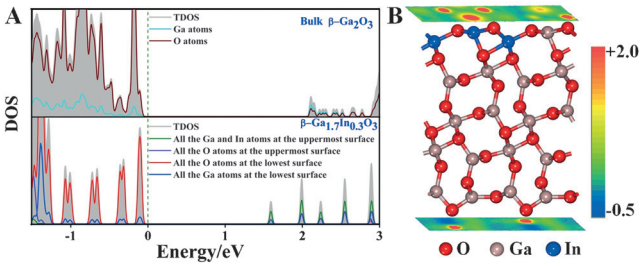

Figure 4. A) Computed density of states (DOS) of β-$Ga_{1.7}In_{0.3}O_3$ with five atomic layers and bulk β-Ga_2O_3. Note that the band gap values determined by density functional theory-based computations are usually smaller than those determined by experiments.[9] B) Electrostatic potentials of the uppermost and lowest surfaces of β-$Ga_{1.7}In_{0.3}O_3$.

Besides the decrease in band gap, an unexpected band structure is observed in $Ga_{1.7}In_{0.3}O_3$ (Figure 4 A). Specifically, the bottom of the conduction band (BCB) and the top of the valence band (TVB) in the material are distributed at the two opposite sides of the ultrathin nanosheets. While the BCB is mainly composed of In and Ga atoms, the TVB is mainly composed of O atoms. However, this unique electronic structure in $Ga_{1.7}In_{0.3}O_3$ may have to do with the ultrathin nanostructure rather than the In dopants present in it, because the same type of electronic structure is also observed in β-Ga_2O_3 possessing 5 atomic layers (Supporting Information, Figure S13).

Owing to its unique band structure, the photogenerated electron–hole pairs formed in $Ga_{1.7}In_{0.3}O_3$ upon photoexcitation can reside at the two outermost surfaces of the material, facilitating the separation of electron–hole pairs. Furthermore, the structure can minimize the barriers that the

electrons and holes have to overcome to make it through from the sites at which they are generated to the sites at which they catalyze the reactions. Additionally, the computed results reveal that the upper surface of $Ga_{1.7}In_{0.3}O_3$ has a higher electrostatic potential than the lower surface (Figure 4B), indicating the existence of an internal electric field between the upper and lower surfaces. This electric field can further aid with the separation of electron–hole pairs because it can inhibit their potential recombination. This is confirmed by transient photovoltage measurement with UV irradiation, which shows that the photovoltage response of $Ga_{1.7}In_{0.3}O_3$ is much higher than that of pristine β-Ga_2O_3 (Supporting Information, Figure S14).

Given their porous nanostructure, ultrathin pore walls and advantageous electronic structure for catalysis, the $Ga_xIn_yO_3$ nanofibers synthesized above are expected to serve as good photocatalysts. As a proof-of-concept, their photocatalytic activity toward room temperature hydrogen evolution reaction (HER) from water using methanol as a sacrificial reagent is measured (see the Supporting Information for details). To evaluate their intrinsic photocatalytic activity, co-catalysts, which are often used with conventional β-Ga_2O_3-based materials,[6,7] are avoided in our case. First, two control reactions, without a photocatalyst or light, are performed. As expected, in both cases no HER is detected. Next, the effect of Ga:In atomic ratio used to synthesize the materials on the rate of HER is examined (Supporting Information, Figure S15), and two conclusions can be made from the results: 1) when the Ga:In atomic ratio is $< 1.2{:}0.8$, the materials do not show photocatalytic activity toward HER; this is because these materials mainly adopt a cubic In_2O_3 crystal structure, whose conduction band edges are lower than the H^+/H_2 potential; 2) when the Ga:In atomic ratio is $> 1.6{:}0.4$, all the materials show significant photocatalytic activity for HER; in particular, the material with Ga:In = 1.7:0.3 gives the best catalytic activity.

Figure 5A shows the photocatalytic HER in the presence of $Ga_{1.7}In_{0.3}O_3$ for 25 h under UV light with intermittent evacuation every 5 h. The result displays a stable hydrogen evolution at a rate of 2295 $\mu mol\,h^{-1}\,g^{-1}$, which is about three times higher than the value obtained for Ga_2O_3 (850 $\mu mol\,h^{-1}\,g^{-1}$). As expected, In_2O_3 does not show photocatalytic activity. The apparent quantum efficiency (AQE) of $Ga_{1.7}In_{0.3}O_3$ measured by using a 313 nm band-pass filter is ca. 3.9%.

To further assess the photocatalytic activity of $Ga_{1.7}In_{0.3}O_3$, three Ga_2O_3-based control materials, namely $Ga_{1.7}In_{0.3}O_3$-NP (NP stands for nanoparticles), Ga_2O_3-NP, and α-β-Ga_2O_3 are synthesized (see the Supporting Information for synthetic details). Both $Ga_{1.7}In_{0.3}O_3$-NP and Ga_2O_3-NP adopt a β-Ga_2O_3 structure, with a porous structure comprising circa 5 nm nanoparticle aggregates (Supporting Information, Figures S16 and S17). They both have a BET surface area is about 40 $m^2\,g^{-1}$. α-β-Ga_2O_3, whose BET surface area is 18 $m^2\,g^{-1}$, is synthesized according to a previous report (Supporting Information, Figure S18).[7a] This material is a highly active photocatalyst owing to its mixed-phase junction, which helps the separation of electron–hole pairs.[7a] A comparison of the mass and specific activities of

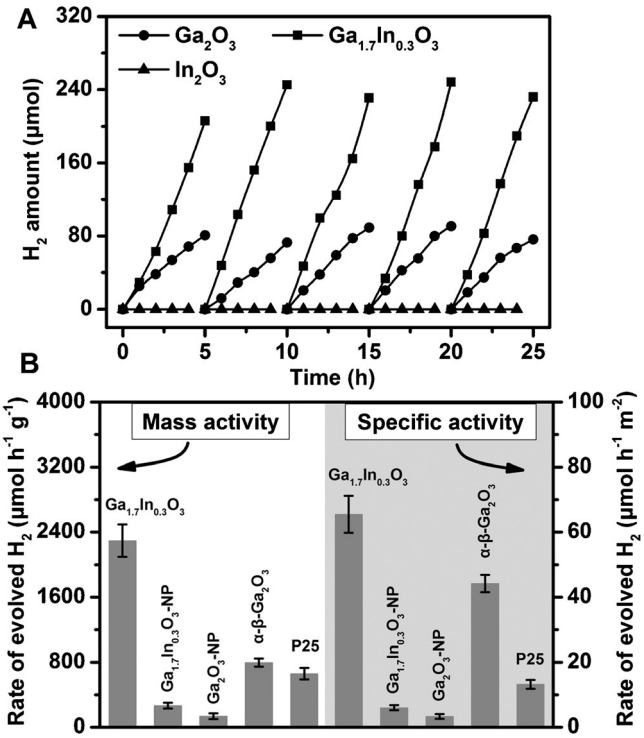

Figure 5. A) HER photocatalyzed by $Ga_{1.7}In_{0.3}O_3$, Ga_2O_3, and In_2O_3 under UV light irradiation. B) Comparative rates of HER over $Ga_{1.7}In_{0.3}O_3$, $Ga_{1.7}In_{0.3}O_3$-NP, Ga_2O_3-NP, α-β-Ga_2O_3, and TiO_2 (P25) under UV irradiation. The error bars represent standard deviations based on five measurements.

the different control materials with respect to that of $Ga_{1.7}In_{0.3}O_3$ is shown in Figure 5B. The mass and specific activities are obtained by normalizing the rate of hydrogen evolution with respect to the mass and BET surface area, respectively, of the material. The mass and specific activities of $Ga_{1.7}In_{0.3}O_3$ are at least 8 times higher than those of $Ga_{1.7}In_{0.3}O_3$-NP, and the mass and specific activities of $Ga_{1.7}In_{0.3}O_3$-NP are about 2 times higher than those of Ga_2O_3-NP. These results indicate that In-doping is not the only reason behind the superior photocatalytic activity exhibited by $Ga_{1.7}In_{0.3}O_3$. In other words, the unique electronic structure in $Ga_{1.7}In_{0.3}O_3$, owing to its unusual nanostructure, must have also contributed to the superior photocatalytic activity of the material. On the other hand, the mass activity of $Ga_{1.7}In_{0.3}O_3$ is 3 times higher than that of α-β-Ga_2O_3, suggesting that the highly porous nanostructure and high surface area of the former may have partially accounted for its excellent photocatalytic activity. It is worth adding that $Ga_{1.7}In_{0.3}O_3$ also exhibits > 3 times higher mass and specific catalytic activities than TiO_2 (P25), which is one of the most common UV photocatalysts.

In conclusion, a porous Ga and In containing bimetallic oxide nano-photocatalyst with atomically thin pore walls has been synthesized. The material has a unique electronic structure that is highly useful for photocatalysis, as demonstrated here with its ability to efficiently photocatalyze the HER. The findings may provide new insights into the fundamental chemistry and physics of atomically thin nano-

structures, and could open a door for the rational design of other highly active nanophotocatalysts.

Acknowledgements

This work is financially supported by the NSFC (21371070, 21401066, 21103065, 21373099, 51572106 and 21573090), the Ministry of Education of China (20110061120024 and 20130061110020), Science and Technology Research Program of Education Department of Jilin Province ([2016] No. 465, [2015] No. 410), and Jilin Province Science and Technology Development Plan (20150101005JC, 20150520003JH). D.W. thanks the National Basic Research Program of China for the financial assistance (2013CB632403). T.A. acknowledges the financial assistance of the US NSF, Grant No.: DMR-1508611.

Keywords: bimetallic oxides · electronic structure · hydrogen evolution reaction · photocatalysis · porous structure

How to cite: *Angew. Chem. Int. Ed.* **2016**, *55*, 11442–11446
Angew. Chem. **2016**, *128*, 11614–11618

[1] a) J. R. Swierk, T. E. Mallouk, *Chem. Soc. Rev.* **2013**, *42*, 2357; b) B. Wu, D. Liu, S. Mubeen, T. T. Chuong, M. Moskovits, G. D. Stucky, *J. Am. Chem. Soc.* **2016**, *138*, 1114; c) P. Li, Y. Zhou, Z. Zhao, Q. Xu, X. Wang, M. Xiao, Z. Zou, *J. Am. Chem. Soc.* **2015**, *137*, 9547; d) S. Ghasimi, S. Prescher, Z. J. Wang, K. Landfester, J. Yuan, K. A. I. Zhang, *Angew. Chem. Int. Ed.* **2015**, *54*, 14549; *Angew. Chem.* **2015**, *127*, 14757.

[2] a) A. L. Linsebigler, G. Lu, J. T. Yates, *Chem. Rev.* **1995**, *95*, 735; b) N. Wu, J. Wang, D. N. Tafen, H. Wang, J. Zheng, J. P. Lewis, X. Liu, S. S. Leonard, A. Manivannan, *J. Am. Chem. Soc.* **2010**, *132*, 6679; c) M. Kitano, M. Hara, *J. Mater. Chem.* **2010**, *20*, 627.

[3] a) M. Kapilashrami, Y. Zhang, Y. Liu, A. Hagfeldt, J. Guo, *Chem. Rev.* **2014**, *114*, 9662; b) K. Zhao, L. Zhang, J. Wang, Q. Li, W. He, J. J. Yin, *J. Am. Chem. Soc.* **2013**, *135*, 15750; c) K. Maeda, M. Eguchi, W. J. Youngblood, T. E. Mallouk, *Chem. Mater.* **2009**, *21*, 3611.

[4] a) S. W. Boettcher, T. E. Mallouk, F. E. Osterloh, *J. Mater. Chem. A* **2016**, *4*, 2764; b) Y. Yu, J. Zhang, X. Wu, W. Zhao, B. Zhang, *Angew. Chem. Int. Ed.* **2012**, *51*, 897; *Angew. Chem.* **2012**, *124*, 921; c) S. Zhuo, Y. Xu, W. Zhao, J. Zhang, B. Zhang, *Angew. Chem. Int. Ed.* **2013**, *52*, 8602; *Angew. Chem.* **2013**, *125*, 8764.

[5] X. Li, Z. Li, J. Yang, *Phys. Rev. Lett.* **2014**, *112*, 018301.

[6] a) H. Park, J. H. Choi, K. M. Choi, D. K. Lee, J. K. Kang, *J. Mater. Chem.* **2012**, *22*, 5304; b) A. Bazzo, A. Urakawa, *Catal. Sci. Technol.* **2016**, *6*, 4243; c) Y. Sakata, Y. Matsuda, T. Nakagawa, R. Yasunaga, H. Imamura, K. Teramura, *ChemSusChem* **2011**, *4*, 181.

[7] a) X. Wang, Q. Xu, M. Li, S. Shen, X. Wang, Y. Wang, Z. Feng, J. Shi, H. Han, C. Li, *Angew. Chem. Int. Ed.* **2012**, *51*, 13089; *Angew. Chem.* **2012**, *124*, 13266; b) X. Wang, S. Shen, S. Jin, J. Yang, M. Li, X. Wang, H. Han, C. Li, *Phys. Chem. Chem. Phys.* **2013**, *15*, 19380; c) T. Liu, I. Tranca, J. Yang, X. Zhou, C. Li, *J. Mater. Chem. A* **2015**, *3*, 10309; d) Y. Sakata, Y. Matsuda, T. Yanagida, K. Hirata, H. Imamura, K. Teramura, *Catal. Lett.* **2008**, *125*, 22.

[8] D. D. Edwards, P. E. Folkins, T. O. Mason, *J. Am. Ceram. Soc.* **1997**, *80*, 253.

[9] J. Paier, M. Marsman, K. Hummer, G. Kresse, I. C. Gerber, J. G. Ángyán, *J. Chem. Phys.* **2006**, *125*, 249901.

Received: June 1, 2016
Revised: June 30, 2016
Published online: August 16, 2016

